Brazilian Dental Journal (2017) 28(1): 97-104
http://dx.doi.org/10.1590/0103-6440201701035

ISSN 0103-6440

Characterization of Conventional and High-Translucency Y-TZP Dental Ceramics Submitted to Air Abrasion

Bhenya Ottoni Tostes[1], Renato Bastos Guimarães[2], Jaime Dutra Noronha-Filho[1], Glauco dos Santos Botelho[1], José Guilherme Antunes Guimarães[1], Eduardo Moreira da Silva[1]

[1]Analytical Laboratory of Restorative Biomaterials – LABiom-R, Dental School, UFF - Universidade Federal Fluminense, Niterói, RJ, Brazil
[2]Physics Institute, UFF - Universidade Federal Fluminense, Niterói, RJ, Brazil

Correspondence: Dr. Eduardo Moreira da Silva, Rua Mário Santos Braga, nº 30 - Campus Valonguinho, Centro, 24020-140 Niterói, RJ, Brasil. Tel: +55-21-2629-9832. e-mail: emsilva@vm.uff.br

This study evaluated the effect of air-abrasion on *t*→*m* phase transformation, roughness, topography and the elemental composition of three Y-TZP (Yttria-stabilized tetragonal zirconia polycrystal) dental ceramics: two conventional (Lava Frame and IPS ZirCad) and one with high-translucency (Lava Plus). Plates obtained from sintered blocks of each ceramic were divided into four groups: AS (as-sintered); 30 (air-abrasion with 30 μm Si-coated Al_2O_3 particles); 50 (air-abrasion with 50 μm Al_2O_3 particles) and 150 (air-abrasion with 150 μm Al_2O_3 particles). After the treatments, the plates were submitted to X-ray diffractometry; 3-D profilometry and SEM/EDS. The AS surfaces were composed of Zr and *t* phases. All treatments produced *t*→*m* phase transformation in the ceramics. The diameter of air-abrasion particles influenced the roughness (150>50>30>AS) and the topography. SEM analysis showed that the three treatments produced groove-shaped microretentions on the ceramic surfaces, which increased with the diameter of air-abrasion particles. EDS showed a decrease in Zr content along with the emergence of O and Al elements after air-abrasion. Presence of Si was also detected on the plates air-abraded with 30 μm Si-coated Al_2O_3 particles. It was concluded that irrespective of the type and diameter of the particles, air-abrasion produced *t*→*m* phase transformation, increased the roughness and changed the elemental composition of the three Y-TZP dental ceramics. Lava Plus also behaved similarly to the conventional Y-TZP ceramics, indicating that this high translucency ceramic could be more suitable to build monolithic ceramic restorations in the aesthetic restorative dentistry field.

Key Words: Y-TZP dental ceramic, air-abrasion, SEM/EDS, X-ray diffractometry, 3-D profilometry

Introduction

Due to their excellent mechanical properties, Y-TZP dental ceramics are among the most widely used framework materials in the field of restorative dentistry. In addition to the mechanical properties, the favorable optical behavior allows this ceramic material to be used as a framework for all types of ceramic restorations, e.g., total crowns, onlays and fixed prosthodontic appliances as well. Y-TZP dental ceramics are composed by a metastable tetragonal phase (*t*), retained at room temperature by careful control of grain size (<0.5 μm) and stabilizer (Y_2O_3) concentration (2-5 mol%) (1). During stress experience, a tetragonal-monoclinic (*t*→*m*) phase transformation takes place at the crack tips under applied stresses, which is accompanied by a volume expansion of about 3–5% (2). This stress-induced *t*→*m* phase transformation leads to the development of internal compressive stresses that oppose crack propagation, creating a toughening mechanism that increases the crack propagation strength of the material (3,4).

In addition to the mechanical behavior, the bond between the ceramic and the tooth tissues is crucial to the service life of indirect restorations. The most used protocol for luting glass ceramic restorations involves dissolving the glass phase of the ceramic by etching it with hydrofluoric acid. However, the absence of silica in their structure renders Y-TZP ceramic materials not susceptible to hydrofluoric acid etching. To overcome this limitation, approaches such as air-abrasion, treatment with gas plasma, silica coating, use of phosphate monomers and fusing glass beads have been suggested to modify the Y-TZP ceramic surfaces in order to achieve strong and reliable bond strengths with the resin cements (5,6).

Air-abrasion is the most used protocol for creating a microretentive surface in Y-TZP dental ceramics. This technique involves hitting the ceramic surface with Al_2O_3 or Si-coated Al_2O_3 particles at high speed, thereby creating a roughened surface with improved wettability (7). Moreover, due to the metastability, the tetragonal phase of Y-TZP ceramics is prone to martensitic *t*→*m* transformation under the stresses produced by air abrasion (2) and this mechanism is able to improve the mechanical properties of the material (8,9). Many published studies analyzed the effect of shape, size and chemical composition of the air-abrasion particles on the surface of Y-TZP dental ceramics (9,10). However, there is still little information regarding the

effect of air-abrasion on elemental composition, roughness, topography and phase transformation of different Y-TZP dental ceramics. Moreover, considering that air-abrasion particles with different sizes are available on the market, it seems of some relevance to evaluate jointly if they could cause dissimilar effects to the different Y-TZP ceramics.

Lava Plus is a recently launched Y-TZP dental ceramic that, according to its manufacturer (3M ESPE), presents high translucency, indicated for zirconia frameworks and monolithic zirconia restorations for anterior and posterior teeth. Although a previous study proved that this ceramic material really presents high translucency (11), to the best of the authors' knowledge there are no available data regarding the effect of air-abrasion on its structure. Therefore, the purpose of this study was to analyze the effect of air-abrasion with different particles on phase transformation, roughness, topography and elemental composition of different types of Y-TZP dental ceramics by X-ray diffractometry, 3-D profilometry and SEM-EDS analysis. The null hypothesis tested was that there would be no difference in the properties among the three Y-TZP dental ceramics.

Material and Methods

The schematic setup of the experiment is in Figure 1. Pre-sintered blocks of three Y-TZP dental ceramics: Lava Frame (LF) and Lava Plus (LP), (3M ESPE, Seefeld, Germany) and IPS ZirCad (IZ), (Ivoclar Vivadent, Schaan, Liechtenstein) were sectioned using a diamond disk (Isomet 1000; Buehler, Lake Bluff, IL, USA) in order to produce 20 plates (10 mm x 10 mm x 2 mm) for each ceramic. After sinterization according to each manufacturer's instructions, the plates were ultrasonicated in distilled water for 5 min, polished with 600-, 1200- and 4000-grit SiC abrasive paper (DPU-10; Struers, Ballerup, Denmark). The plates were randomly divided into four groups (n=5) according to the following surface treatments: AS: as-sintered surface; 30: air-abrasion with 30 μm Si-coated Al_2O_3 particles (Rocatec Plus, 3M ESPE, Seefeld, Germany); 50: air-abrasion with 50 μm Al_2O_3 and 150: air-abrasion with 150 μm Al_2O_3 particles. The three treatments were applied orthogonally to the ceramic surfaces at a pressure of 2.5 bar for 15 s at a 10 mm distance. After the treatments, the plates were ultrasonicated in distilled water for 5 min and air-dried in a glass desiccator containing freshly dried silica gel.

X-ray Diffractometry

The plates were analyzed by X-ray diffraction (XRD) before and after the surface treatments. The used diffractometer was a Bruker AXS D8 Advance (Cu K_a radiation, 40 kV and 40 mA), operating in a Bragg-Brentano Θ/Θ configuration. The diffraction patterns were collected in a flat geometry with 0.0194 degree steps and 0.5 s per step accumulation time, using a PSD detector (Bruker AXS LynexEye). The XRD data were refined following the Rietveld method using GSAS-II software (12). The crystalline phases in the samples were identified with the International Centre for Diffraction Data (ICDD) database by the Match! 1.11f Software.

3-D Profilometry

The topographic analysis was performed using a 3D profilometer (Form Talysurf 60i; Taylor Hobson, Leicester,

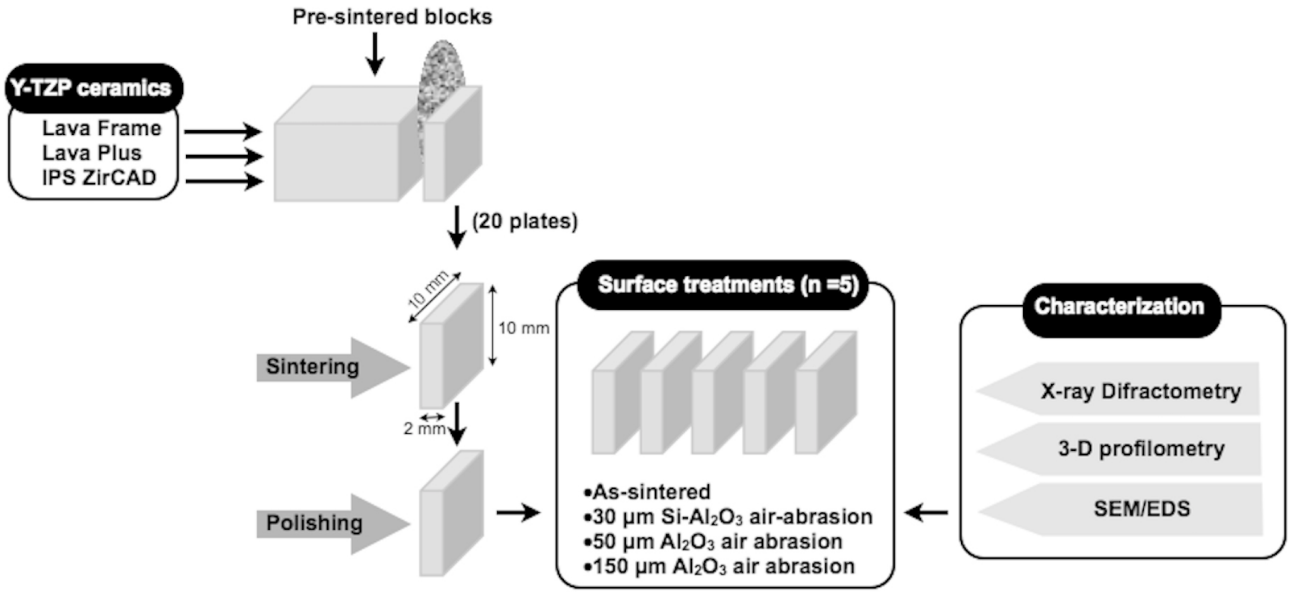

Figure 1. Schematic setup of the experiment.

UK). The plates were scanned with a 20 nm z-resolution, employing 40,000 steps in the x-axis and a spacing of 2 μm in the y-axis. The roughness of the 3D reconstructed images was obtained using the 3-D Sa (average absolute deviation of the surface) and *Sv* (maximum valley depth) parameters, using the following equations:

$$Sa = \frac{1}{A}\iint_A |Z(x,y)|dxdy,$$

$$Sv = \min(Z(x,y))$$

Where Z is the height of the measured point in the coordinates x and y.

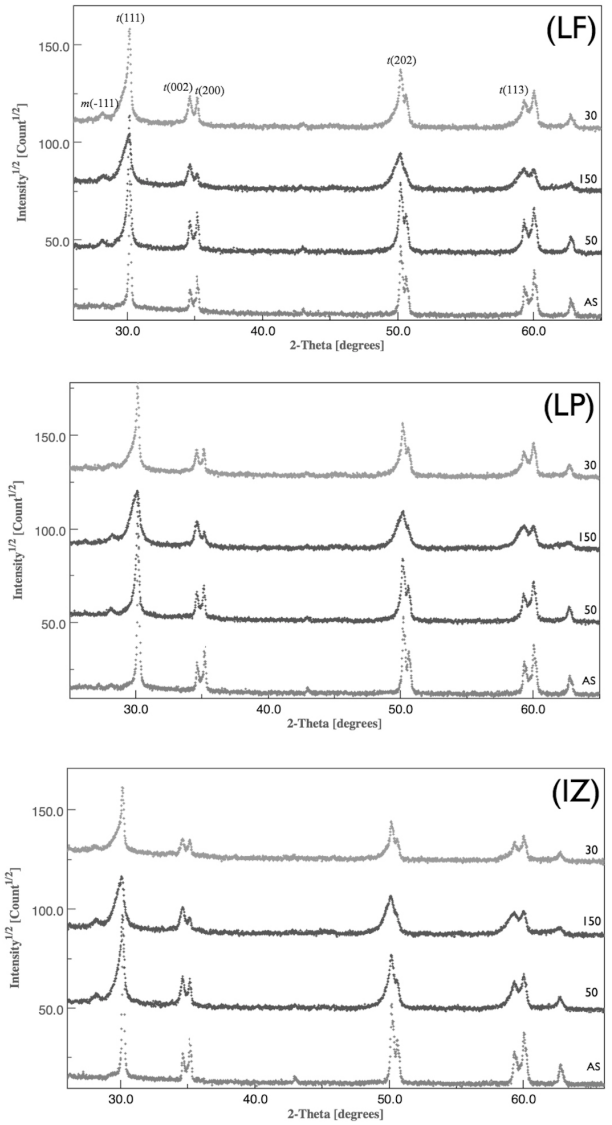

Figure 2. Representative X-ray diffraction patterns of the three Y-TZP dental ceramics submitted to all experimental conditions. (LF) Lava Frame; (LP) Lava Plus and (IZ) IPS ZirCad. (AS) as-sintered surface; (30) 30 μm Si-coated Al_2O_3; (50) 50 μm Al_2O_3 and (150) 150 μm Al_2O_3.

SEM/EDS Analysis

The elemental composition analysis of the three Y-TZP ceramics before (as-sintered) and after air-abrasion was made by energy-dispersive X-ray spectroscopy (EDS). The plates were fixed on aluminum stubs, sputter coated with Au-Pd and observed by SEM (JSM-6510LV; JEOL, Tokyo, Japan) operating in the secondary electron and EDS modes at 20 KV. The SEM image amplification was 2000×. The used EDS system was the THERMO Scientific NSS v 2.1.

The relative intensity of each X-ray line in the EDS spectrum is approximately proportional to the mass concentration of the corresponding element. The system applies a procedure called ZAF, in which corrections for atomic number (Z), absorption (A) and fluorescence (F) effects are calculated from physical models. In this way, the software automatically calculated the wt.% of each detected element (13,14).

Results

X-ray Diffractometry

Figure 2 shows representative X-ray diffraction patterns for the three Y-TZP ceramics submitted to all experimental conditions. On as-sintered surfaces (AS) the three ceramics presented only *t*-phase peaks: (111), (002), (200), (202) and (113), indicating that the materials are tetragonal in nature. After all surface treatments, the (111), (202) and (113) peaks presented an asymmetric broadening. These peaks also presented a remarkable decrease in their intensities in the 150 Group. A new peak emerged at around 28° (-111) and was detected after the three surfaces treatments. There was a clear reversion in the intensities of peaks (002) and (200) in the 150 group.

The wt.% of each phase identified by X-ray diffractometry is presented in Table 1. Before the surface treatments, the three Y-TZP ceramics presented 100% *t* phase (Zr 0.95 Y 0.065 O 1.96). After surface treatments, the three Y-TZP ceramics presented an emergence of the *m* (ZrO_2) and *c* (Zr 0.72 Y 0.0628 O 1.862) phases. On the surfaces treated with 30 μm Si-coated Al_2O_3, LP presented the lowest amount of *m* phase (5.78 wt.%), whereas LF showed the highest (10.26 wt.%). Regarding the *c* phase, the highest amount was presented by LP (28.01 wt.%). IZ was the only ceramic where SiO_2 was identified after this surface treatment (4.64 wt.%). In surfaces air abraded with 50 μm Al_2O_3, the three ceramics presented *m* phase amounts close to each other (2.18 to 3.82 wt.%). On the contrary, IZ showed a remarkable presence of *c* phase (23.65 wt.%) compared to LF (7.52 wt.%) and LP (16.5%). Similarly, in the 150 group, there were no remarkable differences in *m* phase among the three ceramics (7.14 to 11.38 wt.%), but the content of *c* phase presented by LF (36.43 wt.%) was seven- and two-fold greater than those of IZ (5.11 wt.%)

and LP (16.18 wt.%), respectively.

3-D Profilometry

The roughness data were analyzed using two-way analysis of variance and Tukey's HSD test (α=0.05). The mean values and standard deviations for all groups are in Table 2. For both parameters (*Sa* and *Sv*), the roughness was influenced by the air-abrasion particle size, with a significant increase in roughness for particles from 30 to 150 μm ($p<0.05$). Excepting the *Sv* value of LF treated with 30 μm Si-coated Al_2O_3 particles, all other experimental groups presented significantly higher roughness than the as-sintered surfaces ($p<0.05$). Considering the experimental groups (30, 50 and 150), the lowest *Sa* and *Sv* values were presented by LF treated with 30 μm Si-coated Al_2O_3 particles ($p<0.05$). The highest *Sa* and *Sv* values were, respectively, presented by IZ and by LF and IZ after air-abrasion with 150 μm Al_2O_3 particles ($p<0.05$).

Figure 3 shows representative 3-D reconstructed images of the three Y-TZP ceramics. It may be noted that although the roughness increased from the as-sintered surfaces to air-abraded surfaces with 150 μm Al_2O_3 particles, the three Y-TZP ceramics presented a flattened topography, without grooves, after 150 μm Al_2O_3 air-abrasion.

SEM/EDS Analysis

The elemental composition (wt.%) of the three Y-TZP ceramics before and after the surface treatments is shown in Table 3. The AS surfaces of the three ceramics were predominantly composed by Zr (86.73 to 90.10%) and O (5.65 to 9.97%), with traces of Y (1.76 to 3.28%). After the surface treatments, the three ceramics presented an emergence of Al. On air-abraded surfaces with 30 μm Si-coated Al_2O_3, LP presented the highest amount of Al (10.03 wt.%), whereas LF (2.99 wt.%) and IZ (3.6 wt.%) presented a similar content of this element. Si was also identified, ranging from 0.40 to 1.10 wt.% in this group, with LP presenting the highest concentration (1.10 wt.%). In the group air-abraded with 50 μm Al_2O_3, the highest Al emergence was presented by LF (9.16 wt.%), followed by IZ (6.41 wt.%) and LP (5.44 wt.%). In the 150 group, Al ranged from 10.05 to 12.14 wt.%, without remarkable differences among all three Y-TZP ceramics.

Representative SEM images showing the topography of the three Y-TZP ceramics before and after the surface treatments are in Figure 4. The three treatments produced groove-shaped microretentions on the ceramic surfaces, increasing with the diameter of air-abrasion particles. Dispersed Si inclusions are evident on the LF air-abraded surface with 30 μm Si-coated Al_2O_3 particles.

Table 1. Phase composition (wt.%) of the three Y-TZP dental ceramics identified by X-ray Diffractometry

File	$Zr_{0.95}Y_{0.065}O_{1.96}$	ZrO_2	$Zr_{0.72}Y_{0.28}O_{1.862}$	SiO_2
PDF	78-1808	78-0047	77-2115	76-0912
Crystal System	Tetragonal	Monoclinic	Cubic	Tetragonal
Spatital Group	P42/nmc	P21/c	Fm-3m	P43212
		AS		
LF	100	-	-	-
LP	100	-	-	-
IZ	100	-	-	-
		30		
LF	82.22	10.26	7.51	-
LP	66.21	5.78	28.01	-
IZ	83.53	6.48	5.35	4.64
		50		
LF	88.65	3.82	7.52	-
LP	80.39	3.10	16.50	-
IZ	74.17	2.18	23.65	-
		150		
LF	52.19	11.38	36.43	-
LP	72.85	10.97	16.18	-
IZ	87.79	7.14	5.11	-

Discussion

The main goal of this study was to analyze

Table 2. Means (SD) of roughness parameters (μm) of the three Y-TZP dental ceramics

Group	S_a				S_v			
	AS	30	50	150	AS	30	50	150
LF	$0.25^{a,A}$ (0.02)	$0.47^{a,B}$ (0,02)	$0.70^{a,C}$ (0.01)	$1.10^{a,D}$ (0,02)	$2.82^{a,A}$ (0,37)	$2.80^{a,A}$ (0,15)	$4.38^{a,B}$ (0.36)	$7.27^{a,b,C}$ (0,98)
LP	$0.3^{b,A}$ (0.012)	$0.73^{b,B}$ (0.05)	$1.37^{b,C}$ (0.2)	$0.96^{b,D}$ (0.11)	$1.87^{b,A}$ (0.21)	$3.77^{b,B}$ (0.29)	$7.89^{b,C}$ (0.65)	$6.54^{a,C}$ (0.53)
IZ	$0.36^{c,A}$ (0.01)	$1.08^{c,B}$ (0.01)	$0.99^{c,C}$ (0.02)	$1.69^{c,D}$ (0.09)	$3.7^{c,A}$ (0.28)	$5.24^{c,B}$ (0.61)	$5.08^{a,B}$ (0.39)	$8.57^{b,C}$ (1.00)

In columns, means followed by the same lowercase letter are similar (Tukey HSD, $p>0.05$). In rows, for each roughness parameter, means followed by the same uppercase letter are similar (Tukey HSD, $p>0.05$)

the effect of air-abrasion using different size particles on phase transformation, roughness, topography and elemental composition of different types of Y-TZP dental ceramics: two conventional (Lava Frame and IPS ZirCad) and one with high-translucency (Lava Plus). All these aspects play a crucial role on the behavior of Y-TZP ceramic indirect restorations in the oral environment (15). Since Lava Plus behaved similarly to the other analyzed materials , the null hypothesis of the present study was accepted.

Table 3. Elemental composition (wt.% - SEM-EDS) of the three Y-TZP dental ceramics

	O	Y	Zr	Al	Si
			AS		
LF	9.97 (1.70)	3.28 (0.69)	86.73 (1.24)	-	-
LP	5.65 (0.87)	3.25 (0.59)	91.10 (1.07)	-	-
IZ	8.14 (0.99)	1.76 (0.64)	90.10 (1.17)	-	-
			30		
LF	12.41 (2.49)	8.08 (2.23)	75.99 (3.91)	2.99 (0.19)	0.54 (0.18)
LP	18.99 (2.44)	7.74 (2.84)	62.41 (4.44)	10.03 (0.33)	1.10 (0.25)
IZ	7.55 (2.71)	8.70 (3.06)	79.74 (5.32)	3.60 (0.23)	0.40 (0.24)
			50		
LF	11.64 (1.23)	7.67 (1.51)	71.51 (2.88)	9.16 (0.12)	-
LP	25.65 (1.40)	2.54 (0.81)	78.23 (1.76)	5.44 (0.17)	-
IZ	18.53 (1.45)	0.56 (0.37)	74.49 (1.23)	6.41 (0.16)	-
			150		
LF	22.25 (1.65)	4.90 (1.92)	60.70 (3.74)	12.14 (0.25)	-
LP	32.85 (1.86)	4.65 (2.08)	51.33 (3.29)	11.17 (0.23)	-
IZ	17.27 (2.33)	7.06 (2.79)	65.61 (5.18)	10.05 (0.22)	-

The amount of *m* phase identified after air-abrasion, ranging from 2.18 to 11.38 wt.% (Table 1) nicely agrees with previous studies (2,10). The emergence of *m* phase may be seen in Figure 2, where, for the three Y-TZP ceramics a $t \rightarrow m$ transformation is clear, characterized by a reduction in the intensity and broadening of the *t*-phase peaks (111) at an angle of 31˚, and the appearance of the left *m*-phase peak (-111) at an angle of approximately 28˚. Moreover, it is noteworthy that the intensity of this *m*-phase peak (-111) increased with the diameter of the Al_2O_3 used for air-abrading the material surface. This finding may be explained by the permanent lattice distortions induced by the increasing mechanical action produced by the impact of the Al_2O_3 particles on the material surface (10,16). Another important aspect seen in Figure 2 is the reversion in the intensities of the (002) and (200) peaks after abrading with 150 μm Al_2O_3 particles. This behavior has been linked to the ferroelasticity of Y-TZP ceramics, indicating that more residual stresses were triggered on the materials surface (2,16). According to Monaco et al. (16), this change in the intensity of these diffraction peaks may cause an additional increase in the fracture toughness of the Y-TZP ceramics because the application of tensile stress, as found at the tip of an advancing crack, can cause domain

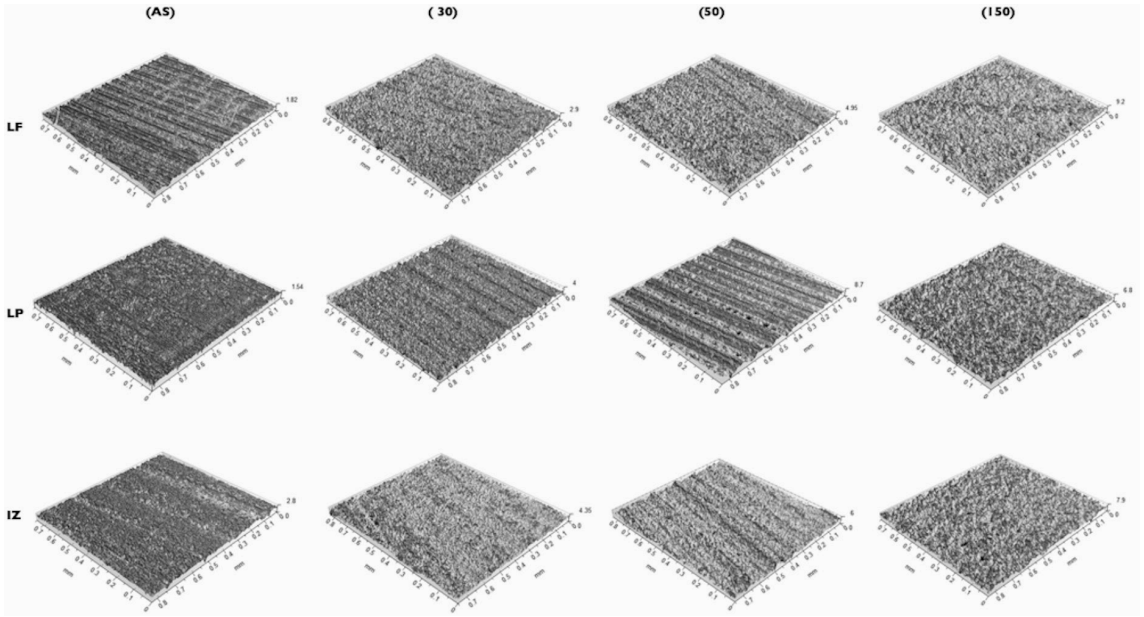

Figure 3. Representative 3-D reconstructed images of the three Y-TZP dental ceramics submitted to all experimental conditions. (LF) Lava Frame; (LP) Lava Plus and (IZ) IPS ZirCad. (AS) as-sintered surface; (30) 30 μm Si-coated Al_2O_3; (50) 50 μm Al_2O_3 and (150) 150 μm Al_2O_3 (α and β angles=45°/z axis in μm).

reorientation and the absorption of fracture energy without phase transformation.

All these aspects prove that the induction of *t*→*m* phase transformation was greater after air-abrasion with 150 μm Al_2O_3 (Table 1). Hallmann et al. (10) also showed that the greater the Al_2O_3 particles, the higher the stress-induced *t*→*m* phase transformation on Y-TZP ceramic surfaces, claiming that this depended on the coarseness of air-abrasion particles. This behavior was also demonstrated in other previous studies (17,18). Moreover, Özcan et al. (8) showed that Al_2O_3 particles are rougher than Si-coated Al_2O_3 particles. This aspect may also have influenced the *t*→*m* phase transformation produced by 150 μm Al_2O_3 particles in the present study. In view of the influence of grain size, the greater *t*→*m* phase transformation produced by 30 μm Si-coated Al_2O_3 compared to 50 μm Al_2O_3 was unexpected and it is not easy to explain. However, this behavior was also found by Yamaguchi et al. (19), who showed that 30 μm Si-coated Al_2O_3 produced greater *t*→*m* phase transformation than 70 μm Al_2O_3. Also, Özcan et al. (8) did not find differences in the relative amount of *m* phase after abrasion with 30 μm Si-coated Al_2O_3 and 50 μm Al_2O_3.

Since many studies published in this field have shown that as-sintered Y-TZP ceramics are predominantly composed of the tetragonal phase but also present a low content of cubic phase (3,9), it was a surprise that no cubic phase was detected in as-sintered specimens in the present study (Table 1). The first explanation of this may be based on differences in the microstructural characteristics of the used Y-TZP ceramics, such as grain size, yttria content and initial phase composition, and those used in those cited studies. Second, Matsui et al. (20) proposed the grain boundary segregation-induced phase transformation (GBSIPT) model to explain the *t*→*c* transformation during sintering of Y-TZP ceramics. This model states that, during the initial and intermediate steps of sintering (≅1300 °C), a microstructure of monophasic tetragonal and grain-boundary segregation of Y^{3+} is formed. When the sintering temperature increases (≅1500 °C), the widths of Y^{3+} ions segregated in grain boundaries and triple junctions increase inside grain interiors with grain growth, and then regions with high Y^{3+} concentrations are formed in grain interiors. These regions with high Y^{3+} ion concentrations change into the cubic phase by *t*→*c* transformation. However, analyzing ultra-pure Y-TZP powder containing 3 mol% yttria, Chevalier et al. (21) found a dual microstructure (*t* and *c* phases) only when the ceramic powder was sintered at 1550 °C for 5 h. Based on this, the authors supposed that the maximum temperature used to sintering the Y-TZP ceramics in the present study (1500 °C), was not sufficient to induce *t*→*c* transformation, and so the cubic phase was not identified in as-sintered specimens. The results of Pereira et al. (22), who did not find *c* phase in as-sintered Y-TZP ceramics may reinforce this possibility.

On the other hand, the *c* phase was detected in the three Y-TZP ceramics after all surface treatments (Table 1). Moreover, the final level of *c* phase (5.11 to 36.43 wt.%) was higher than that of *m* phase (2.18 to 11.38

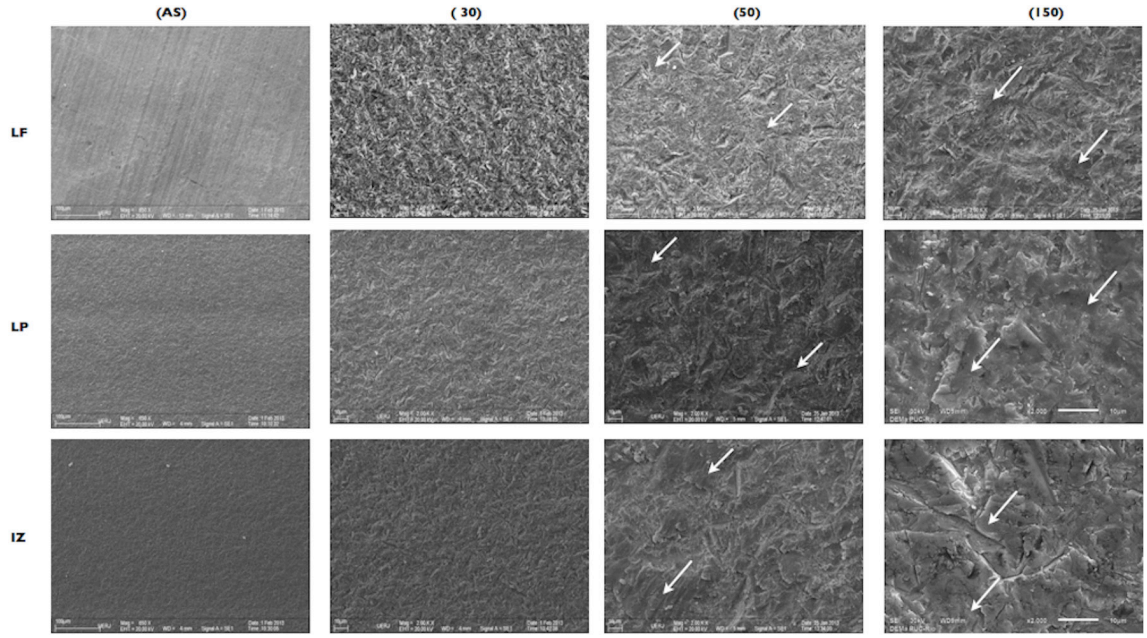

Figure 4. Representative SEM images of the three Y-TZP dental ceramics submitted to all experimental conditions. (LF) Lava Frame; (LP) Lava Plus and (IZ) IPS ZirCad. (AS) as-sintered surface; (30) 30 μm Si-coated Al_2O_3; (50) 50 μm Al_2O_3 and (150) 150 μm Al_2O_3. White arrows indicate areas of permanent plastic deformation on the ceramic surfaces.

wt.%), (Table 1). Using Vickers indentation to induce phase transformation in a Y-TZP ceramic, Pittayachawan et al. (3) showed that the *t*→*m* transformation was more prominent in areas of tensile and shear stresses, whereas the *t*→c transformation occurred in the center of the indentation, where compressive stress was higher. Thus, since air-abrasion produces more compressive stress than tensile and shear stresses, it is expected that the presence of c phase could be higher than *m* phase after air-abrasion.

The *Sa* roughness parameter expresses the average of the absolute values of Z(x,y) in the measured area, equivalent to the arithmetic mean of the measured region on the 3D display diagram when valleys changed to peaks by conversion to absolute values. However, this parameter only supplies a general measure of surface texture and it is insensitive to differentiate peaks, valleys and spacing of various texture features. On the other hand, the *Sv* parameter, which expresses the maximum valley depth Zv on the surface in the measured area, can supply a more useful information regarding resin-based cement retention to the ceramic surfaces. These data are crucial, because it is well established that air-abrasion increases surface roughness, thereby improving the reliability of adhesion between Y-TZP dental ceramics and the resin-based cements (23).

The information depicted in Table 2 shows that, for both parameters, the roughness increased with the diameter of the air-abrasion particles. This finding supports those of Turp et al. (17), who showed an increase in roughness from 0.62 to 0.91 μm after air-abrasion with 30 μm Si-coated, 50 μm and 110 μm Al_2O_3 particles. From the clinical point of view, this increase in roughness can positively affect the adhesion between Y-TZP dental ceramics and resin-based cements by two ways. First, an increase in surface roughness means that a superficial layer rich in organic contaminants that reduce the wettability of the ceramic surface, is removed. Thus, the interaction between the materials (ceramic and resin-based cement) could be more effective. Second, the increased surface area and deep valleys produced by air-abrasion on ceramic surfaces will create more sites of retention available to the *in situ* polymerization of the resin-based cement (17,24).

Although the roughness increased with increasing air-abrasion particle diameter, analysis of Figure 3 shows that the grooves produced by polishing the ceramic surfaces with SiC abrasive papers were smoothed or eliminated after air-abrasion with 150 μm Al_2O_3 particles. This aspect is noteworthy because it indicates that these surfaces tend to be flattened, even when presenting a higher *Sa* and *Sv* roughness. Such topography may contribute to reduce the stress concentration in the adhesive interface between ceramic and resin-based cement. Moreover, Scherer et al. (9) claimed that besides the classic stress-induced *t*→*m* phase transformation toughening, the smoothening of the ceramic surfaces produced by air-abrasion with 30 μm silica-coated Al_2O_3 particles could also contribute to the improvement of fatigue behavior of Y-TZP ceramics. Thus, although the mechanical behavior was not investigated in the present study, it is reasonable to claim that the smoothness surfaces produced after air-abrasion with 150 μm Al_2O_3 particles (Fig. 3) could positively influence the mechanical properties of Y-TZP ceramics. Certainly, this possibility requires further confirmation.

The SEM/EDS analysis showed that air-abrasion produced alterations in the elemental composition of the Y-TZP dental ceramics (Table 3). For the three groups, a decrease in Zr content along with the emergence of Al ranging from 2.99 to 12.14 wt.% was detected. This finding is remarkable because these values are far greater than the content of Al_2O_3 normally included in the composition of Y-TZP ceramics (≅0.25%). According to Hallmann et al. (10), the kinetic energy of the air-abrasion particles is released in form of thermal energy, thereby causing a local melting of the ceramic surface that can include the particles. Thus, the increased Al and O content detected here could be explained by the inclusion of Al_2O_3 particles onto the ceramic surfaces. Moreover, the values depicted in Table 3 show that the higher the diameter of the air-abrasion particles, the greater the alterations in elemental composition. Most probably, this is due to the greater surface abrasion produced by the larger abrasive particles, i.e., 50 and 150 μm Al_2O_3. The aspects seen in Figure 3, where more areas of permanent plastic deformation are present in the 50 and mainly the 150 groups (white arrows), may reinforce this explanation.

In the ceramic surfaces air-abraded with 30 μm Si-coated Al_2O_3 particles, SEM/EDS analysis also detected an emergence of a low content of Si, ranging from 0.40 to 1.10 wt.%. According to Hallmann (10), the kinetic energy of the silica-coated alumina particles is also converted to atom vibration energy of the ZrO_2 lattice, leading to the breaking of the Zr-O-Zr bonds. This favors the chemical reaction between Zr and Si and could produce a melted zirconium silicate nanolayer on the ceramic surface.

Analyzing the aging resistance of Y-TZP dental ceramics, Inokoshi et al. (25) showed that the microstructure and the grain size of Lava Frame, Lava Plus and IPS ZirCad were quite similar. This is corroborated by the results of the present study, in which the elemental compositions of these ceramic materials were found to be in the same range (Table 3), and could be used to explain why there were no remarkable differences in the properties presented by the three Y-TZP dental ceramics

evaluated here.

Three methods of air-abrasion produced *t→m* phase transformation, increased the roughness, modified the topography and changed the elemental composition of the three Y-TZP dental ceramics. However, these modifications were more effective after air-abrasion with 150 μm Al_2O_3 particles. Therefore, clinically, the 150 μm Al_2O_3 particles seem to be more suitable to treat the internal surfaces of Y-TZP dental ceramic indirect restorations. Also, the recently introduced Y-TZP dental ceramic (Lava Plus) behaved similarly to the other ceramics analyzed here. Taking into account its high translucency, this may represent an advantage to this material, indicating that this ceramic is more suitable to build monolithic ceramic restorations in the field of aesthetic restorative dentistry.

Resumo

Este estudo avaliou o efeito da abrasão a ar na transformação de fase *t→m*, na rugosidade, topografia e composição elementar de três cerâmicas Y-TZP (Zircônia tetragonal policristalina estabilizada por **ítrio**): duas convencionais (Lava Frame e ZirCad) e uma de alta translucidez (Lava Plus). Placas obtidas de blocos sinterizados de cada cerâmica foram divididos em quatro grupos: AS (pré-sinterizado); 30 (jateamento com partículas de Al_2O_3 de 30 μm cobertas com Si); 50 (jateamento com partículas de Al_2O_3 de 50 μm) e 150 (jateamento com partículas de Al_2O_3 de 150 μm). Após os tratamentos, as placas foram submetidas à difratometria de Rx, perfilometria 3-D e microscopia eletrônica de varredura com espectroscopia de energia dispersiva de Rx (SEM/EDS). As superfícies pré-sinterizadas apresentaram predominantemente Zr e fase tetragonal.

Todos os tratamentos superficiais produziram transformação *t→m* nas cerâmicas avaliadas. A topografia e a rugosidade foram influenciadas pelo diâmetro das partículas abrasivas (150>50>30>AS). A análise através de SEM mostrou que os três tratamentos produziram fendas retentivas nas superfícies das cerâmicas, por influência do tamanho das partículas. A análise através de EDS mostrou uma diminuição da concentração de Zr, paralela ao surgimento de O e Al, após o jateamento. No grupo tratado com partículas de Al_2O_3 de 30 μm cobertas com Si foi também observado um aumento de Si após o jateamento. Concluiu-se que, independente do tipo e do diâmetro das partículas, o jateamento produziu transformação *t→m*, aumentou a rugosidade e alterou a composição elementar das cerâmicas avaliadas. A Lava Plus apresentou comportamento semelhante às cerâmicas convencionais, indicando que esta cerâmica de alta translucidez pode ser mais adequada à confecção de restaurações monolíticas no campo da odontologia estética restauradora.

References

1. Kelly JR, Denry I. Stabilized zirconia as a structural ceramic: an overview. Dent Mater 2008;24:289-298.
2. Chintapalli RK, Marro FG, Jimenez-Pique E, Anglada M. Phase transformation and subsurface damage in 3Y-TZP after sandblasting. Dent Mater 2013;29:566-572.
3. Pittayachawan P, McDonald A, Young A, Knowles JC. Flexural strength, fatigue life, and stress-induced phase transformation study of Y-TZP dental ceramic. J Biomed Mater Res B Appl Biomater 2009;88:366-377.
4. Tong H, Tanaka CB, Kaizer MR, Zhang Y. Characterization of three commercial Y-TZP ceramics produced for their high-translucency, high-strength and high-surface area. Ceram Int 2016;42:1077-1085.
5. Martins AR, Gotti VB, Shimano MM, Borges GA, Goncalves LS. Improving adhesion between luting cement and zirconia-based ceramic with an alternative surface treatment. Braz Oral Res 2015;29:1-2.
6. Hallmann L, Ulmer P, Wille S, Polonskyi O, Kobel S, Trottenberg T, et al.. Effect of surface treatments on the properties and morphological change of dental zirconia. Journal of Prosthetic Dentistry 2016;115:341-349.
7. Heikkinen TT, Lassila LV, Matinlinna JP, Vallittu PK. Effect of operating air pressure on tribochemical silica-coating. Acta Odontol Scand 2007;65:241-248.
8. Ozcan M, Melo RM, Souza RO, Machado JP, Felipe Valandro L, Bottino MA. Effect of air-particle abrasion protocols on the biaxial flexural strength, surface characteristics and phase transformation of zirconia after cyclic loading. J Mech Behav Biomed Mater 2013;20:19-28.
9. Scherrer SS, Cattani-Lorente M, Vittecoq E, de Mestral F, Griggs JA, Wiskott HW. Fatigue behavior in water of Y-TZP zirconia ceramics after abrasion with 30 μm silica-coated alumina particles. Dent Mater 2011;27:e28-42.
10. Hallmann L, Ulmer P, Reusser E, Hammerle CH. Surface characterization of dental Y-TZP ceramic after air abrasion treatment. J Dent 2012;40:723-735.
11. Wang F, Takahashi H, Iwasaki N. Translucency of dental ceramics with different thicknesses. J Prosthet Dent 2013;110:14-20.
12. Larson AC, Von Dreele RB. General Structure Analysis System (GSAS). Los Alamos National Laboratory 2004; Report LAUR 86-748.
13. Scott VD, Love G. Quantitative Electron Probe Microanalysis. 2nd ed Ellis Horwood, Chichester 1994.
14. Goldstein J. Scanning Electron Microscopy and X-ray Microanalysis. Springer Science + Business Media, New York 2003.
15. Traini T, Gherlone E, Parabita SF, Caputi S, Piattelli A. Fracture toughness and hardness of a Y-TZP dental ceramic after mechanical surface treatments. Clin Oral Investig 2014;18:707-714.
16. Monaco C, Tucci A, Esposito L, Scotti R. Microstructural changes produced by abrading Y-TZP in presintered and sintered conditions. J Dent 2013;41:121-126.
17. Turp V, Sen D, Tuncelli B, Goller G, Ozcan M. Evaluation of air-particle abrasion of Y-TZP with different particles using microstructural analysis. Aust Dent J 2013;58:183-191.
18. Passos SP, Linke B, Major PW, Nychka JA. The effect of air-abrasion and heat treatment on the fracture behavior of Y-TZP. Dent Mater 2015;31:1011-1021.
19. Yamaguchi H, Ino S, Hamano N, Okada S, Teranaka T. Examination of bond strength and mechanical properties of Y-TZP zirconia ceramics with different surface modifications. Dent Mater J 2012;31:472-480.
20. Matsui K, Horikoshi H, Ohmichi N, Ohgai M, Yoshida H, Ikuhara Y. Cubic-formation and grain-growth mechanisms in tetragonal zirconia polycrystal. J Am Ceram Soc 2003;86:1401-1408.
21. Chevalier J, Deville S, Munch E, Jullian R, Lair F. Critical effect of cubic phase on aging in 3 mol% yttria-stabilized zirconia ceramics for hip replacement prosthesis. Biomaterials 2004;25:5539-5545.
22. Pereira GK, Amaral M, Simoneti R, Rocha GC, Cesar PF, Valandro LF. Effect of grinding with diamond-disc and -bur on the mechanical behavior of a Y-TZP ceramic. J Mech Behav Biomed Mater 2014;37C:133-140.
23. da Silva EM, Miragaya L, Sabrosa CE, Maia LC. Stability of the bond between two resin cements and an yttria-stabilized zirconia ceramic after six months of aging in water. J Prosthet Dent 2014;112:568-575.
24. Sarmento HR, Campos F, Sousa RS, Machado JP, Souza RO, Bottino MA, et al.. Influence of air-particle deposition protocols on the surface topography and adhesion of resin cement to zirconia. Acta Odontol Scand 2014;72:346-353.
25. Inokoshi M, Vanmeensel K, Zhang F, De Munck J, Eliades G, Minakuchi S, et al.. Aging resistance of surface-treated dental zirconia. Dent Mater 2015;31:182-194.

Received May 11, 2016
Accepted September 6, 2016